Experimental results on convective heat transfer of an air-flow through a wavy channel

L. Colombo, A. Muzzio, A. Niro*
Dipartimento di Energetica, Politecnico di Milano
Piazza Leonardo da Vinci, 32 I-20133 Milano, Italy
**corresponding author. E-mail: alfonso.niro@polimi.it*

Abstract
The paper presents an experimental analysis on forced-convection heat transfer characteristics inside a rectangular channel with the lower and upper walls corrugated, at Reynolds number between 500 and 6300. The channel is 200 mm wide and 10 mm high; corrugations have a triangular cross-section, 20 mm wide and 2.68 mm high, arranged perpendicular to the streamwise direction, which alternate staggered of half a pitch on the lower and upper walls. Local heat transfer characteristics are investigated by non-intrusive measurements of velocity and temperature fields by LDV and real time holographic interferometry, respectively; data on average convection coefficient, and apparent Darcy friction factor are also reported. Waviness significantly improves heat transfer; the enhancement factor, in fact, is nearly 1.6 in laminar regime, while it starts to quickly increase with the Reynolds number as the flow becomes transitional (Re≈1370), coming up to 4 at Re=6300. This enhancement, however, is strongly penalized by a 700% incresase of the friction factor.

1. Introduction

Wavy fins are an efficient and cost-effective solution to enhance heat transfer of air-flows inside compact heat-exchangers with extended surfaces. In fact, due to small passages and relatively low air velocity, flow is laminar or weakly turbulent and convective coefficient is low. Specially configured extended-surfaces, such as offset strip, louvered, perforated, and wavy, are widely used because they provide quite larger convection transfer rates. This performance improvement is essentially due to the alteration of duct fluid-dynamic rather than to the increase of heat transfer area. Many enhancement mechanisms can be used but those most frequently employed are periodic deflection of streamlines, periodic interruptions of the boundary layer growth and flow destabilization. Furthermore, these specially configured extended-surfaces also promote turbulence development, as the corrugation size is close to that of the fluid dynamic structures to be excited (the lower the Reynolds number, the larger these structures). Because of the large variety of possible shapes and geometries, there is a large number of studies in the open literature. For instance, Webb [1] reports more than 35 papers and almost as many are cited by Fiebig [2]. For offset strip fin geometry, correlations for predicting the Colburn and friction factors were proposed by Kays [3], Joshi and Webb [4], and Wieting [5]; similar correlations were developed by Davenport [6] for louvered fin geometry. Finally, wavy fin geometry is also the subject of some interesting studies, such as those by Goldstein and Sparrow [7], and Ali and Ramadhyani [8]), but there are not quite general correlations for this geometry because of a rather lacking data base. For these motivations, we are currently performing an experimental and numerical investigation on flows through channels with wavy walls.
This paper reports on local and average heat transfer coefficients, and pressure drops of an air-flow through a wavy channel at Reynolds numbers within the typical operating range of extended surfaces heat-exchangers. Corrugations have a triangular cross-section, with the apex on one wall coinciding with the throw on the other wall, which induce a periodic streamline deflection.

2. Experiments

The experimental setup, that is schematically shown in Figure 1, is composed of the air circuit containing the test channel and the heating water circuit. The test channel has a rectangular cross

section of 200 mm in width and 10 mm in height, it is horizontally positioned and is constituted by entry, test and exit sections (test section is only qualitatively depicted in the figure). Room air flows into the entry section through an opening with rounded surfaces; the entry section is a 1 m long, that is 55 times the hydraulic diameter, and its walls are not heated; at the end of this section, fully developed flow conditions are reached and air enters the test section. This is 800 mm long with glass windows as side walls to permit viewing of its inside. The top and bottom walls are made with aluminum alloy blocks, 200 mm long, with a cross-section given by superimposing a triangle, 20 mm wide and 2.68 mm high, to a square with a 20 mm side; the blocks are mounted side by side, staggered of half pitch on the top and bottom walls, and strongly tightened between them and to their own heating water channel. In order to monitor wall temperatures of the test-section, six thermocouples are inserted into the lower wall and two into the upper one; all junctions are placed 0.5 mm beneath the channel surface; these thermocouples also provide an accurate reference temperature for the interpretation of the interferograms. Downstream the test section, there are a 0.5 m long exit section, a filter, three float-type flow-meters (nominal accuracy of 2%), a metering valve and a blower operating in suction mode. Eventually, the exhausted air is discharged outside the laboratory. The heating water circuit is mainly composed by a heat bath, which provides a high mass flow rate of water at constant temperature within 0.1 K, and by the channels mounted on the bottom and top walls of the test section, respectively, where the water flows in the opposite direction of the air. These channels have a rectangular cross section, 180 mm wide and 5 mm high, with the wall in contact with the test section manifactured by an aluminum alloy, 12 mm thick plate. Wall temperature differences are within 0.1 K perpendicularly to the flow direction whereas they rise up to 0.8 K along the test section.

Air temperature is measured at the test-section entrance, downstream the filter, and upstream and downstream the flow-meters. Air bulk temperature at the test-section outlet is also measured, but not simultaneously with local thermal measurements; in this case, the exit section is equipped with two rows of turbolizers and with a convergent channel that conveys air flow through a narrow duct (1 cm in width) filled with a tangle of copper fine wires where two thermocouples are embedded. All the thermocouples used are copper-constantan made of 0.25-mm-diameter wire, with the cold junctions in a ice bath; the temperature measurement accuracy is of 0.2 K. The axial component of air velocity is measured along vertical traverses in 20 points each, by laser velocimetry using a TSI system which includes a fiberoptic probe and the IFA750 signal processor; each measurement results from the average of five readings based on a 4096 data sample.

The measurement of temperature fields is obtained by means of real-time holographic interferometry. The interference patterns are electronically recorded by a progressive, monochrome CCD ½" camera, 782x582 pixel resolution, 10 bit dynamic range, and 25 not-interlaced frames per second.

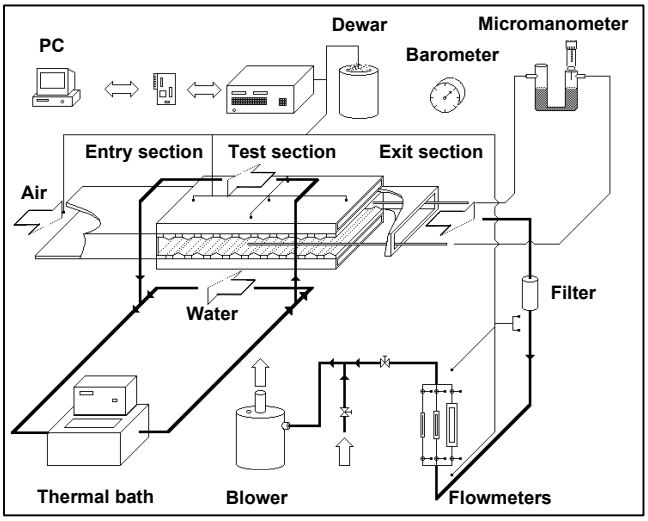

Figure 1. Schematic of the experimental apparatus.

Evaluation of the interferometric images consists in reconstructing the phase-difference distribution from the light-intensity distribution, and it is performed using a phase-shifting method which requires the recording of more interferograms for a given state while shifting the phase of one of the interferometer beams of a time-constant amount, Hariharan [9]. This method is characterized by a sensitivity higher than that of maximum/minimum fringe location method (it is accredited to resolve phase-differences up to one hundredth of the source wave length) but it requires a more complex experimental setup and digital techniques for evaluating interferograms. Once the phase-difference distribution has been determined, the tem-

perature distribution inside the test section and its derivative normal to the wall are evaluated. Data presented here are processed with the Carré method and with an original method developed by one of the authors. The normal derivative is numerically evaluated by using a mesh of 10 pixels. The local Nusselt number is calculated as

$$Nu = \frac{D_h}{T_w - T_b}\left(-\frac{\partial T}{\partial n}\right)_w$$

where $(\partial T/\partial n)_w$ is the temperature normal derivative evaluated at the wall, D_h the hydraulic diameter, T_w the wall temperature, and T_b the air bulk temperature obtained by numerical quadrature from the experimental temperature and velocity distributions. The measurement uncertainty of Nu has been experimentally estimated about 5.6%.
The average Nusselt number over the entire heated channel is evaluated as

$$Nu_{av} = \frac{\rho V c_p D_h}{k A_s}\ln(\theta_i/\theta_o)$$

where V is the volume flow rate of air, ρ the density evaluated at the temperature and pressure where V is measured, c_p the specific heat at constant pressure, k the thermal conductivity, A_s the total area of the heated surface, θ_i and θ_o are the wall to air bulk temperature difference at the entrance and the exit of the channel, respectively. The uncertainty on Nu_{av} measurement, evaluated by a propagation error analysis, is 6% on the average but it becomes larger than 15% when θ_o lowers under 2 °C, namely, at the highest values of Nu_{av}. Finally, pressure drop is measured by means of two probes, each consisting of a 6-mm o.d. tube with two pairs of 0.1-mm-diameter pressure taps on the tip, plugged into the channel; these probes are connected to a differential liquid micromanometer with a 0.125-Pa sensitivity. The apparent Darcy friction factor is calculated as

$$f = \frac{2D_h A^2}{\rho V^2}\frac{\Delta p}{L_{chan}}$$

where Δp is the pressure drop over the entire wavy channel, A and L_{chan} are the cross section area and the length of the channel, respectively. The measurement of this factor is affected by an uncertainty of 5.2% on the average but this comes up to 10% at the lowest values of Δp.

3. Experimental results

The channel investigated in this paper is schematically shown in Figure 2, whereas Table I lists its main geometric parameters. Heat transfer data are obtained keeping the lower and upper walls at the uniform temperature of 70 °C, whereas the measurements of velocity and pressure drop of the air

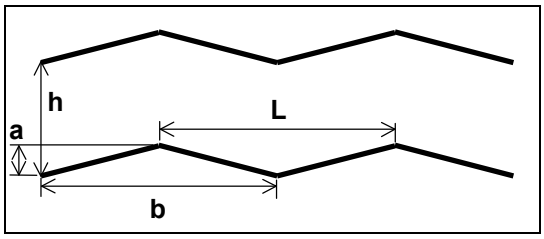

Figure 2. Schematic of the channel section geometry.

h	[mm]	10.00
a	[mm]	2.68
b	[mm]	20.00
L	[mm]	20.00
Vertex angle		150°
Channel width	[mm]	200.00
Hydraulic diameter	[mm]	18.18
Heigth to width ratio		0.05
Ribs number		30

Table 1. Channel geometric characteristics.

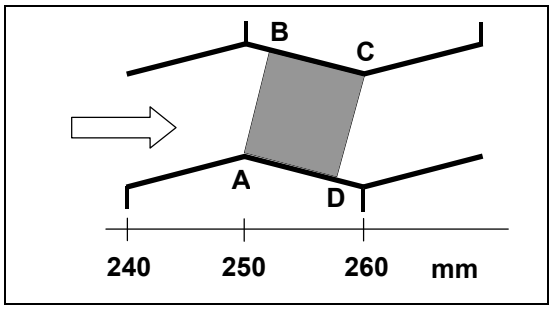

Figure 3. Thermal field measurement region.

flow are performed with channel walls at room temperature because the thermal effects on fluid dynamic are negligible under this temperature difference. In all the tests, air inlet temperature is nearly 20 °C. Local heat transfer measurements are taken around the thirteenth corrugation of the lower wall, namely 215 mm downstream of test section inlet, where flow conditions are periodically fully developed, that is where the velocity and scaled temperature profiles repeat periodically equal over a corrugation cycle length. Figure 3 shows the measurement region; this is rectangular shaped, the vertex A coincides with the apex of the thirteenth lower corrugation at 250 mm from the wavy-channel inlet, the short side is parallel to the corrugation facet, the vertex C falls on the thirteenth upper corrugation at 260 mm from the inlet. Finally, in the scheme air flows from left to right so the lower side AD is leeward whereas the upper side BC is windward.

Figure 4 displays for instance 5 temperature profiles at Re=1082 obtained along as many traverses parallel to region side AB, and equally spaced of 50 pixels each other; abscissa is expressed in pixels with the zero in the vertex B. From the nspection of how profiles evolve in the flow direction, we can observe that the minimum increases for the heating effect, the temperature gradient at the lower wall decreases because we are moving from the corrugation apex to the throat along the leeward facet whereas the gradient at the upper wall increases for the opposite reason. The figure also shows that temperature profiles are affected by larger fluctuations at the wall due to the noise generated by wall diffraction fringes; this broader scatter in temperature data in turn yields a higher uncertainty in evaluating the gradient at the wall and, hence, the local Nusselt number. Figure 5 presents the streamwise distributions of the local Nusselt number along the upper and lower sides of the measurement region for Reynolds number Re=487. As previously noticed, data points are to some extent scattered; to improve result readability, in the figure we reported two curves fitting the data for the lower and upper facets, respectively, obtained by the least-squares method with a polynomial function.

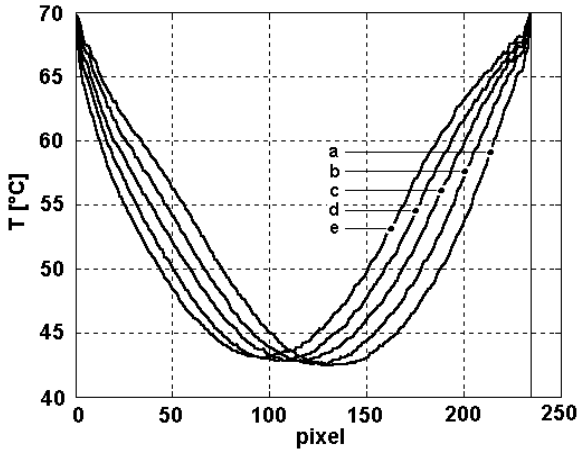

Figure 4. Temperature profiles along 5 traverses, parallel to the AB side, and 50 pixel equally spaced each other. Traverse *a* is taken at 50 pixels apart the vertex A.

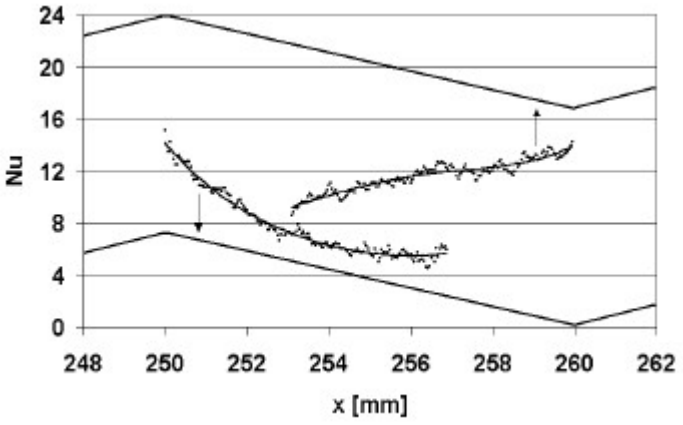

Figure 5. Experimental point dixtribution and interpolated trends of the local Nusselt number at Re=487; arrows point to the facet which points and curve refer to.

To further improve the result readability along a whole corrugation, in Figure 6 the curve fitting the local Nusselt number on the upper side BC is plotted translated of half a pitch, i.e., before that for the lower side AD, as if it had been obtained along the windward facet of the thirteenth lower

corrugation. This transposition is tolerable for thermally fully developed flow and, in the present study, this assumption is supported by strong experimental indications. The trends reported in Figure 6 are for three different Reynolds numbers, i.e., Re=487, Re=1082, and Re=1370. As it can be seen, the trends are quite similar between them, namely the local Nusselt number increases along the windward facet, it reaches a maximum at the corrugation apex with a value up to 2.5 times higher than that for plain channel, after it starts to decrease very quickly first and then more slightly while approaching the corrugation throat. For all three cases, however, the per-module average value of the Nusselt number is 9.7, that is a bit less than 1.5 times the plain-channel value. Finally, for Re=487 the Nusselt number displays a peculiar trend on the leeward facet, i.e., it is characterized by a flex; this trend is confirmed by numerical simulations performed by means of a commercial finite-volume CFD code.

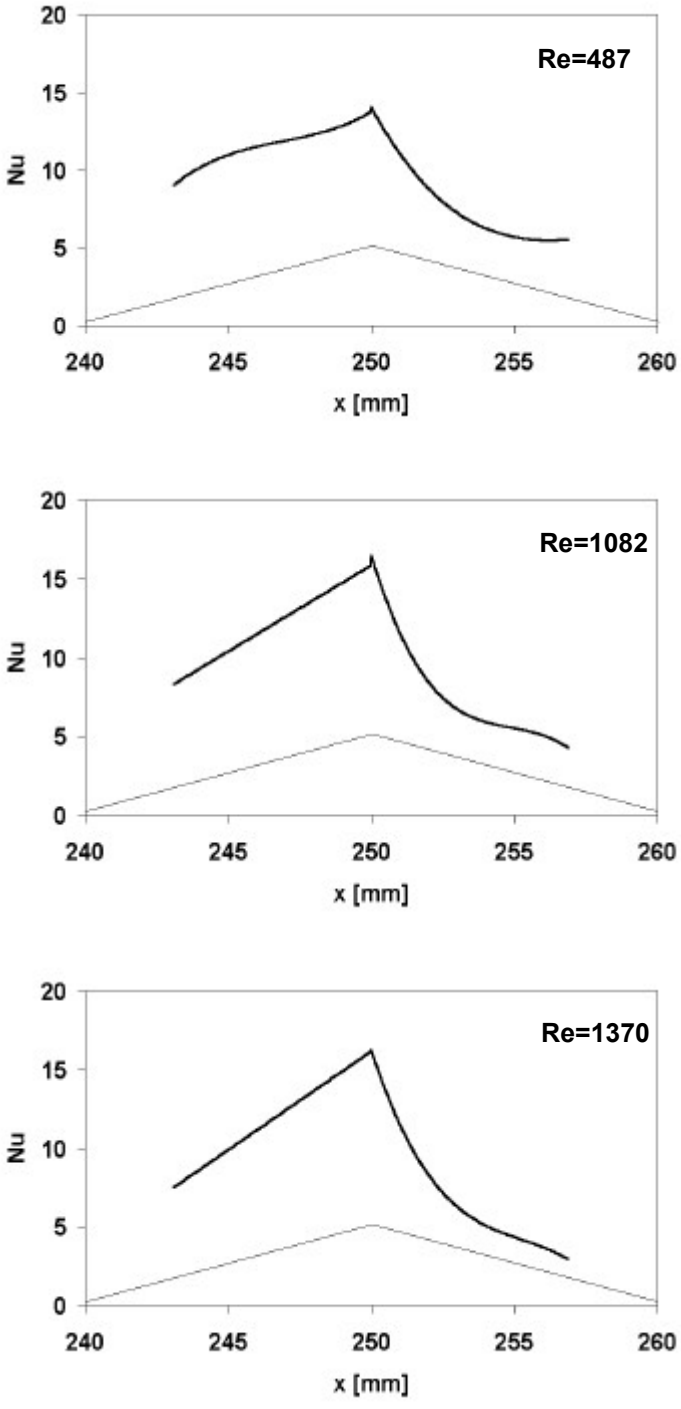

Figure 6. Interpolated trends of the local Nusselt number at three different Re; the first curve branch does not really refers to the lower corrugation but it is obtained on the upper windward facet.

In Figure 7 the average Nusselt number over the entire heated section is plotted versus the Reynolds number; for comparison, the figure also reports the values for a plain channel calculated by the correlations of Shah and London for Re≤2300, and of Gnielinsky for higher values. As seen, for Re≤1370 flow regime is laminar and the average Nusselt number is practically a constant equal to 11.16, that is 67% higher than the plain-channel value; obviously, this value is also larger than the per-module average in the thermally fully developed region, which amounts to 9.7, because it benefits of the entry region. Consequently, waviness considerably alters the local convection coefficient distribution, but the average heat transfer increases to a less extent. In contrast, for Re>1370 the average Nusselt number starts to quickly increase, exhibiting a power-law dependence on the Reynolds number; up to Re=3100, the exponent is 1.43 and after it lowers to 0.8. From this trend we argue the flow regime is transitional for Reynolds numbers between 1370 and 3100 and after it becomes fully turbulent. At Re=6300, corresponding to the upper limit of the investigated range, the average Nusselt number is nearly 80 with an over 400% increase with respect to the plain channel. The conjecture the flow regime becomes transitional at Re=1370 and fully turbulent at Re=3100, is supported by the trend of the air dimensionless-temperature at the exit $T^* = (\theta_{in} - \theta_o)/\theta_{in}$

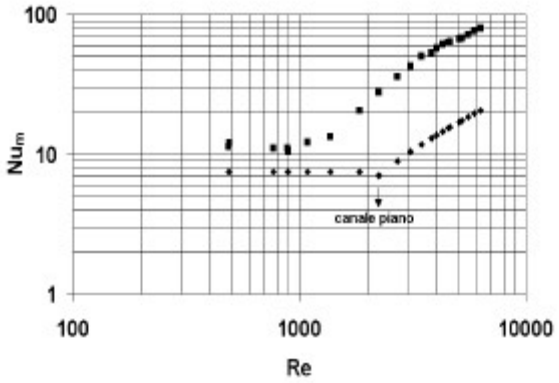

Figure 7. Average Nusselt number vs. Reynolds number; plain channel values are calculated.

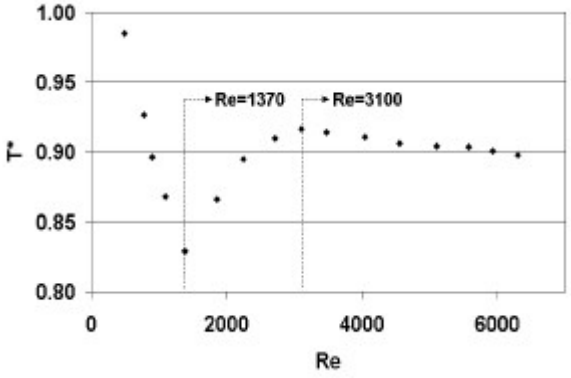

Figure 8. Air dimensionless temperature at the channel outlet vs. Reynolds number.

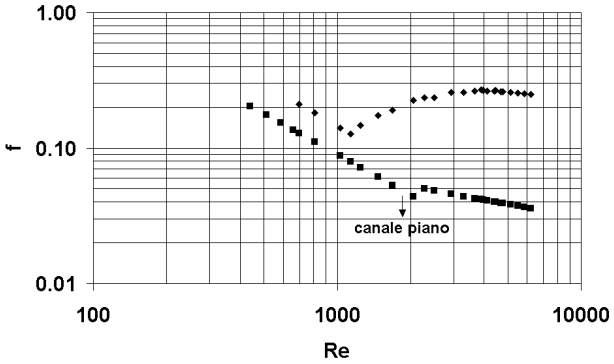

Figure 9. Darcy apparent friction factor vs Reynolds number; experimental values for a plain channel, with the same width but 10 mm high, are also reported for comparison.

that, as shown in Figure 8, presents a minimum at the former value and a maximum at the latter.

Finally, Figure 9 reports the experimental values of the apparent Darcy friction factor plotted versus the Reynolds number for the present channel and, for comparison, for a plain channel with the same width but 15 mm high. The friction factor for the wavy channel displays a trend similar to the plain channel in laminar flow regime but with 60% larger values; when the flow regime becomes transitional, the trend reverses and the friction factor starts to noticeably increase; however, the minimum occurs at a Reynolds number slightly less than that predicted by the dimensionless temperature trend. As the Reynolds number is further increased, the growth attenuates and eventually, when flow is fully developed, the friction factor seems to attain the asymptotic value of 0.25 that is 7 times the plain channel value at Re=6300.

4. Conclusions

This paper reports about an experimental investigation on heat transfer characteristics of an airflow inside a wavy channel at Reynolds numbers between 500 and 6300. The enhancement effect is essentially due to the periodic streamline deflection induced by the wall waviness. The heat transfer measurements over the entire channel show the flow is laminar up to Re=1370; within this regime, the average Nusselt number is independent of the Reynolds number, as for the plain-channel case, but its value is 67% higher; finally, local convection coefficient exhibits very far larger variations with respect to the plain-channel value. In spite to these enhanced heat transfer characteristics, however, the Darcy apparent friction factor worsens of nearly 60%. At Re=1370, flow regime becomes transitional in advance, therefore, with respect to the plain channel. This event is well pointed out by a minimum in the dimensionless temperature trend, as well as by an abrupt slope change in the average Nusselt number trend which from a constant becomes a power-law increasing function of the Reynolds number with an exponent of 1.43; the friction factor trend, however, does not exactly confirm this indication and suggests a slightly lower value of the Reynolds number for the occurrence of this regime. The transitional flow regime is characterized by a strong increase of the heat transfer coefficient and the apparent friction factor with respect to the plain-channel.

Finally, for Re≥3100 flow becomes fully turbulent, the growth of the average Nusselt number with Re attenuates -the exponent of the letter lowers to 0.8, i.e., the characteristic value for plain channel-, and the apparent friction factor seems to asymptotically tend to 0.25. Consequently at Re=6300, i.e., the upper limit of the Re investigated range, the present wavy channel is characterized by an enhancement factor of 4 but with a 700% larger friction factor.

Nomenclature

a	corrugation height, m
b	corrugation length, m
A	channel cross section area, m^2
A_s	total area of the heated surface, m^2
c_p	specific heat at constant pressure, J/kgK
h	channel height, m
k	thermal conductivity, W/mK
D_h	hydraulic diameter, m
L	rib/groove spacing, m
L_{chan}	channel length, m
n	normal to the wall
T_b	air bulk temperature, K
T_w	wall temperature, K
V	volume flow rate of air, m^3/s

Greek symbols

θ	wall to air bulk temperature difference, K
ρ	density, kg/m^3

Subscripts

i	inlet
o	outlet
w	wall

Acknowledgments

This work is supported by MURST (the Italian Ministry for the University and for the Scientific and Technical Research) via COFIN 2002 grants.

References

1. Webb, R.L., *Principles of Enhanced Heat Transfer*, John Wiley & Sons, cap. 9, pp. 228-284, 1994.
2. Fiebig, M., "Vortices: tools to influence heat transfer. Recent developments", Proc. 2nd European Thermal Sciences and 14th UIT National Heat Transfer Conference, vol. 1 pp. 41-56, Rome, June 1996.
3. Kays, W.M., Compact Heat Exchangers, AGARD Lecture Ser. No. 57 on Heat Exchangers, ed. Ginoux, AGARD-LS-57-72, Jan. 1972.
4. Joshi, H.M., Webb, R.L., Prediction of heat transfer and friction in the offset strip fin array, Int. Journal of Heat and Mass Transfer, Vol. 30, No. 1, pp. 69-84, 1987.
5. Wieting, A.R., Empirical correlations for heat transfer and flow friction characteristics of rectangular offset fin heat exchangers, J. Heat Transfer, Vol. 97, pp. 488-490, 1975.
6. Davenport, C.J., Correlations for heat transfer and flow friction characteristics of louvered fin, Heat transfer-Seattle 1983, AIChE Symp. Ser., No. 225, Vol. 79, pp. 19-27, 1984.
7. Goldstein, L.J., Sparrow, E.M., Heat/mass transfer characteristics for flow in a corrugated wall channel, J. Heat Transfer, Vol. 99, pp. 187-195, 1977.
8. Ali, M.M., Ramadhyani, S., Experiments on convective heat transfer in corrugated channels, Experimental Heat Transfer, Vol. 5, pp. 175-193, 1992.
9. Hariharan, P., Optical Holography: principles, techniques, and application, Cambridge University Press, 1995.